Effects of temperature and CO_2 concentration on the early-stage nucleation of calcium carbonate by reactive molecular dynamics simulations

Ling Qin[a,b,c,d], Junyi Yang[a], Jiuwen Bao[a], Gaurav Sant[e], Sheng Wang[c], Peng Zhang[a], Xiaojian Gao[f], Hui Wang[g], Qi Yu [c]*, Ditao Niu[h]*, Mathieu Bauchy[d,e]*

[a] School of Civil Engineering, Qingdao University of Technology, Qingdao 266033, China
[b] Post-doctoral Mobile Stations of Civil engineering, Xi'an University of Architecture & Technology, Xi'an 710055, China
[c] Qingdao Qingjian New Material Group Co., Ltd., Qingdao 266108, China
[d] Physics of AmoRphous and Inorganic Solids Laboratory (PARISlab), Department of Civil and Environmental Engineering,University of California, Los Angeles, California 90095, USA
[e] Institute for Carbon Management (ICM), University of California, Los Angeles, California 90095, USA
[f] School of Civil Engineering, Harbin Institute of Technology, Harbin 150090, China
[g] Ningbo Key Laboratory of Energy Geostructure, Ningbo, 315211, China
[h]Department of Civil Engineering, State Key Laboratory of Green Building in Western China, Xi'an University of Architecture and Technology, Xi'an 710055, China

*Correspondence: yuqi0421@126.com; niuditao@163.com; bauchy@ucla.edu

ABSTRACT

It is significant to investigate the calcium carbonate ($CaCO_3$) precipitation mechanism during carbon capture process, nevertheless, $CaCO_3$ precipitation is not clearly understood yet. Understanding the carbonation mechanism at atomic level can contribute to the mineralization capture and utilization of carbon dioxide, as well as the development of new cementitious materials with high-performance. There are many factors such as temperature, CO_2 concentration can influence the carbonation reaction. In order to achieve better carbonation efficiency, the reaction conditions of carbonation should be fully verified. Therefore, based on the molecular dynamics simulations, this paper investigates the atomic-scale mechanism of carbonation. We investigate effect of the carbonation factors including temperature and concentration on the kinetics of carbonation (polymerization rate and activation energy), the early nucleation of calcium carbonate etc. Then, we analyze the local stresses of atoms to reveal the driving force of early-stage carbonate nucleation and the reasons for the evolution of polymerization rate, activation energy. Results show that the higher the calcium concentration or temperature, the higher the polymerization rate of calcium carbonate. And the activation energies of

carbonation reaction increase with the decrease of calcium concentrations.

I. INTRODUCTION

Since the start of the industrial revolution in the 1760s, atmosphere carbon dioxide (CO_2) concentration has increased significantly[1]. As the principal greenhouse gas, the escalating concentrations of carbon dioxide will lead to the entrapment of solar radiation within the Earth's atmosphere, thus, causing the rise of global temperatures. Global warming has caused significant negative impacts on the environment, such as frequent extreme meteorological events, obvious changes in precipitation patterns, annual expansion of arid areas, and further aggravation of sea level rise[2]. Therefore, how to effectively deal with global climate change, solve the prominent contradiction between economic development and environmental change, and promote sustainable economic and social development has become the top issue for governments of all countries and the attention focus of all the people. Cement concrete is the most widely used construction materials in the world[3-6]. Nevertheless, the cement and concrete industry is a major industrial production source of CO_2 emissions. Ordinary Portland cement (OPC) is the main used cementitious materials in concrete, which accounts for about 10% of the total concrete mass[7]. China is a major cement producer, the global annual OPC production is about 4.2 billion tons, of which more than 60% is produced in China[8]. According to statistics, the production of a ton of cement will produce 0.9~1 ton of carbon dioxide. Cement production accounts for about 9% of global man-made carbon dioxide emissions[9-11]. Consequently, it is imperative to mitigate the carbon footprint of the cement industry. In recent years, carbonation curing has garnered substantial attention as an efficacious method for capturing carbon dioxide and reducing carbon emissions in the construction sector[12-13]. Different from the carbonation erosion in hardened concrete, where carbonation has an adverse effect on concrete performance.

Carbonation curing initiates during the early stages of cement hydration, wherein unhydrated clinker minerals, such as calcium silicate (C_3S, C_2S), and certain hydration products ($Ca(OH)_2$, C-S-H), react with carbon dioxide to generate calcium carbonate[14-15]. The formed calcium carbonate can improve the pore structure, furthermore, to improve the performance of cement concrete[16-19].

There are many factors can influence the carbonation curing. The optimal moisture content is crucial in this process, as low moisture limits carbonation rates, while excessive moisture impedes CO_2 diffusion into the cement matrix. Therefore, maintaining an optimal moisture content is essential for early-age carbonation curing[20]. The pre-curing step, conducted after specimen casting and before CO_2 exposure, significantly influences the initial moisture content and pore structure of the samples[21-23]. Given that early-age carbonation is a diffusion-controlled reaction[24-25], according to Fick's second law, the duration of carbonation and the partial pressure of CO_2 have significant effects on the degree of carbonation. There are some other factors including temperature, relative humidity, CO_2 concentration can influence the carbonation curing[20,26]. The increase of temperature can promote the CO_2 diffusion via accelerating the thermal motion of air molecules and the evaporation of water[20]. However, the higher temperatures can also reduce the solubility of gaseous carbon dioxide. Relative humidity has a similar effect with the water content summarized above, which is usually controlled at about 60~70% during carbonation curing[27-28]. Therefore, in order to achieve better carbonation efficiency, the reaction conditions of carbonation curing should be fully verified.

It is well known that carbonation occurs through a solution-precipitation process. During this process, the solid phase, which includes calcium hydroxide, has the capability to dissolve in an aqueous solution. Subsequently, it reacts with dissolved carbonate to generate an amorphous calcium hydrate precursor known as calcium carbonate gel. The amorphous calcium hydrate precursor will then be

dried and crystallized to form crystalline calcium carbonate[29-31]. As the precursor to the crystalline carbonate phase, comprehending the formation mechanism of calcium carbonate gel is crucial. Nevertheless, prior research has predominantly concentrated on the macroscopic features of carbonated cement, leaving the atomic-scale mechanism of calcium carbonate nucleation inadequately explored[30,32-33]. Gaining insights into the atomic-scale mechanisms of carbonation holds the potential to establish a robust scientific foundation for processes that have traditionally relied on empirical approaches, thus facilitating the development of novel performance-enhanced cementitious materials.

Hence, to unveil the atomic-scale mechanism of carbonation in solidified carbonated cementing materials, we conduct an investigation into the impact of carbonation factors including temperature, CO_2 concentration on the kinetics of carbonation (polymerization rate and activation energy), early nucleation of calcium carbonate through molecular dynamics simulations. Then, we analyze the local stresses of atoms to reveal the driving force of early-stage carbonate nucleation and the reasons for the evolution of polymerization rate, activation energy.

II. METHODS

A. Simulated methodology

The simulation of calcium carbonate hydration gel was carried out using the large-scale atomic/molecular large-scale parallel simulation (LAMMPS) software package[34]. It is common knowledge that the solubility of calcium hydroxide ($Ca(OH)_2$) in cement pore solution is approximately 22×10^{-3} mol/L[35]. Previous experiments utilized a Ca^{2+} concentration range of 0.2×10^{-3} to 2×10^{-3} mol/L to investigate the coordination environment of precursor species Ca^{2+} during the formation of calcium carbonate minerals[36]. Moreover, the simulated components described in reference[37] including 30 Ca^{2+} and 1000 H_2O molecules. Therefore, we adopt a series of Ca^{2+} concentrations from 1.67×10^{-3} mol/L to

11.13×10^{-3} mol/L. The chosen concentration of CO_3^{2-} is in accordance with the concentration of Ca^{2+} to uphold the neutrality of the simulated system. Specific details regarding the molecular composition of the simulation are provided in Table 1.

Table 1 Initial components of simulation system

Ca/H_2O ratio (%)	Ca	CO_3	H_2O
3	30	30	1000
6	30	30	500
10	30	30	300
15	30	30	200
20	30	30	150

The individual Ca^{2+}, CO_3^{2-} and H_2O molecules were randomly positioned within a 40 Å cubic simulation box using the PACKMOL package[38] and the periodic boundary conditions were applied. It is worth noting that unrealistic overlap between the simulation atoms should be avoided. Fig. 1 presents a initial configuration snapshot of the simulation system, H_2O molecules are omitted for clarity. The simulation system is relaxed in an isothermal isobaric (NPT) ensemble for 300 ps through the implementation of a Nosé-Hoover thermostat and a barostat developed by Melchionma et al.[39-40], which is found to be long enough to ensure the convergence of volume, potential energy and pressure of the whole simulation system. In order to investigate the effect of temperature and press on carbonation mechanism, the adopted simulation temperatures include 300K, 325K, 350K, 400K, 450K when the pressure is fixed at 1 atm. And the simulation pressures are 1atm, 10atm, 30atm, 50 atm, 70 atm, 100 atm when the temperature is 300K. Furthermore, the Velocity-Verlet integration algorithm is employed to characterize the motion of atoms, utilizing a time step of 0.25 fs.

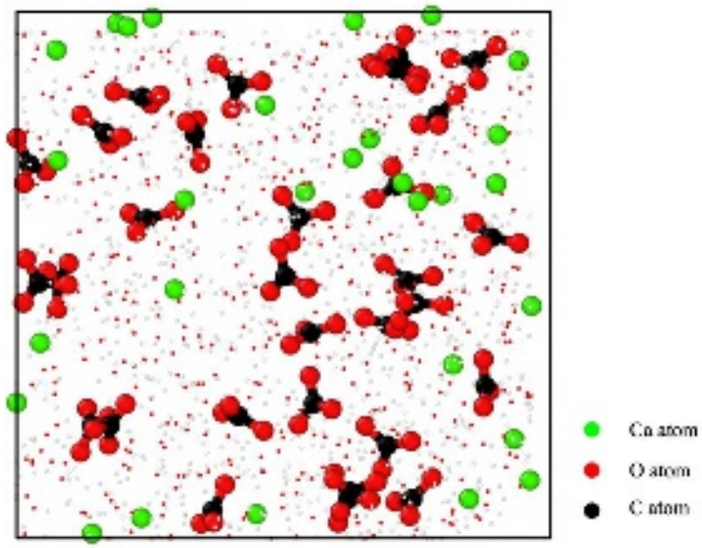

Fig. 1. Initial configuration of the simulated amorphous calcium carbonate system.

B. Simulation forcefields

Our simulation utilizes the reactive forcefield (ReaxFF) parameterized by van Duin et al.[41]. This forcefield has been demonstrated to provide an accurate representation of the time-dependent gelation process of amorphous calcium carbonate systems under aqueous conditions[42]. ReaxFF has garnered increasing attention for its ability to bridge the gap between quantum mechanical calculations and classical molecular dynamics simulations. Unlike classical forcefields, which model atoms as rigid ions with fixed charges, ReaxFF utilizes the charge equilibration (QEq) method[43]. This method dynamically allocates charges to atoms within the ReaxFF framework. The atoms charges and interatomic bond order between atoms are related to the local environment (including atomic radii, electron affinities, etc.) of each atom. According to the adjustment of the energy terms and the calculation of the interatomic bond order, ReaxFF can model the chemical reactions, specifically, describe the breaking/formation of chemical bond. Therefore, ReaxFF can simulate disordered/defected materials and their reactivity[44-45]. During the reactive forcefield simulation, the total energy can be described by the follow equation[46-48]:

$$E_{sys}=E_{bond}+E_{Coulomb}+E_{VdWaals}+E_{under}+E_{lp}+E_{over}+E_{tors}+E_{val}+E_{pen}+E_{conj} \quad (1)$$

Where E_{bond}, $E_{Coulomb}$, $E_{VdWaals}$, E_{under}, E_{lp}, E_{over}, E_{tors}, E_{val}, E_{pen} and E_{conj} represent the short-range bond energy, Coulomb potential energy, Van der Waals energy, under-coordination energy, long-range electron pairs energy, over-coordination energy, torsion energy, valence angle energy, penalty energy and conjugation energy, respectively. Specifically, E_{bond}, E_{tors}, and E_{val} are covalent terms derived from the general relationship between dynamic bond order and interatomic distances. More details about these energy terms are described in the Refs.[47-48].

C. Structural analysis

The atomic topological structure of amorphous calcium carbonate ($CaCO_3$) gels is described by partial coordination number, which is calculated by enumerating the number of adjacent atoms in the first coordination shell. The atomic pair cutoff is determined as the minimum distance after the first peak in the atomic pairs partial pair distribution functions (PDF). We can recognize the Ca-C bond, C-O bond, Ca-O bond in amorphous $CaCO_3$ gels structure based on the atomic pair cutoff. Moreover, according to the identification of these bonds, we can get the evolution of $CaCO_3$ gel network connectivity, the carbonate clusters size and number. The $CaCO_3$ cluster is defined as a group consisting of interconnected O, C, and Ca atoms, and the size of each cluster is determined by counting the number of C atoms belonging to that specific cluster. Ovito software[49] was used for visualization and clustering analysis of the simulation results.

D. Local atomic stress computation

The concept of stress per atom, as proposed by Ekami[50-51], has been employed to assess the local instability present in the atomic network, arising from competing interatomic forces. It should be noted that the stress is a macroscopic property in nature and it is difficult to define the stress for the single

atom[52]. However, as shown in equation (1), based on the contribution to the system dimension, the atomic scale stress tensor ($\sigma_i^{\alpha\beta}$) can be defined for each single atom[53].

$$\sigma_i^{\alpha\beta} = 1/V_i \cdot \Sigma_j r^{\alpha}_{ij} \cdot F^{\beta}_{ij}, \quad (1)$$

where V_i, r_{ij} and F_{ij} denote the voronoi volume of atom i, the distance between atoms i and j, and the interatomic force exerted by atom j on atom i. The superscripts α and β represent the projections of these vectors along the Cartesian directions x, y, or z[30]. Additionally, positive and negative stress values represent the local states of tension and compression, respectively, experienced by an atom. To quantify the internal stresses within stress-rigid atomic networks and mixed-alkali glasses[54-56], the atomic scale stress tensor ($\sigma_i^{\alpha\beta}$) has also been employed.

III. RESULTS AND DISCUSSION

A. Evolution of the network connectivity during gelation

An investigation into the evolution of network connectivity during the gelation of $CaCO_3$ is conducted by examining the connectivity of Ca atoms throughout the gelation process. Specifically, Fig. 2 depicts the partial coordination numbers of Ca-O at a temperature of 300 K and a Ca/H_2O ratio of 3%. In this context, Oc and Ow represent the O atoms belonging to CO_3^{2-} and H_2O, respectively, while Ot denotes the total O in the simulation system (Ot=Ow+Oc). Notably, the average coordination number of Ca atoms (Ca-Ot/Ca) remains relatively stable at 6.8 throughout the gelation process, aligning with previous research findings[30]. Whereas, the type of O atoms within the first coordination shell of Ca atoms undergoes changes over the simulation time. Initially, Ca atoms are entirely surrounded by Ow atoms, indicating that Ca^{2+} starts as an isolated hydrating cation. As the simulation progresses, Ca-Ow bonds are gradually replaced by Ca-Oc bonds, signifying the formation of bonds between Ca atoms and O atoms belonging to CO_3^{2-}. This evolution leads to the appearance of carbonate clusters through the

formation of Ca-Oc-C bonds.

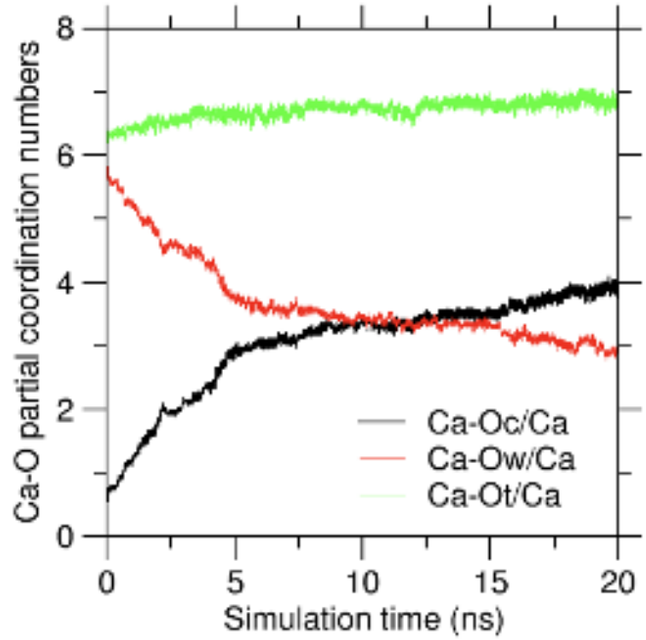

Fig. 2. Ca-O partial coordination numbers at 300K when Ca/H_2O=3%.

Fig. 3 illustrates the number of Ca-Oc links per Ca at various temperatures. It is observed that the Ca-Oc bond number gradually increases with the extension of simulation time and tends to stabilize over time. Additionally, the final number of Ca-Oc bonds increases with higher temperatures when the concentration is constant. This suggests that the final polymerization degree of calcium carbonate gel rises with elevated temperatures. In Fig. 4, the number of Ca-Oc links per Ca is depicted at various calcium concentrations with a fixed temperature of 300K. Notably, concentration exerts a significant influence on the number of Ca-Oc bonds. As calcium concentration increases, the number of Ca-Oc bonds also rises, eventually stabilizing with the extension of simulation time.

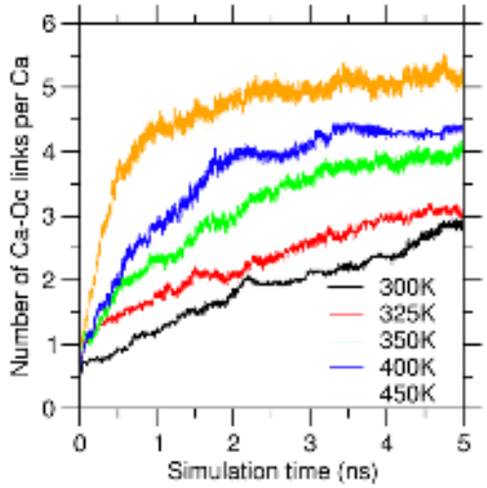

(a) Ca/H_2O=3%

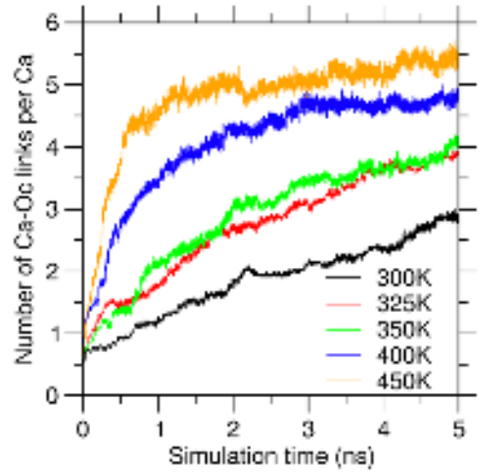

(b) Ca/H_2O=6%

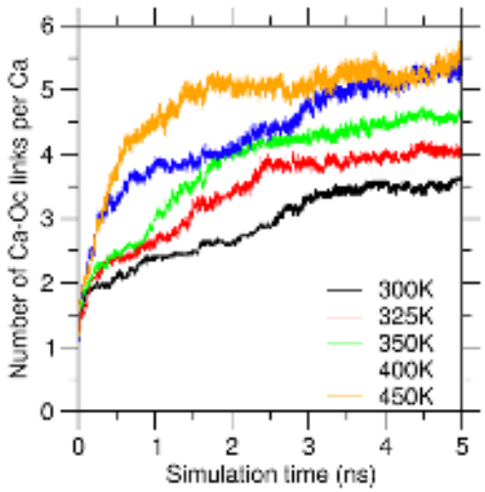

(c) Ca/H_2O=10%

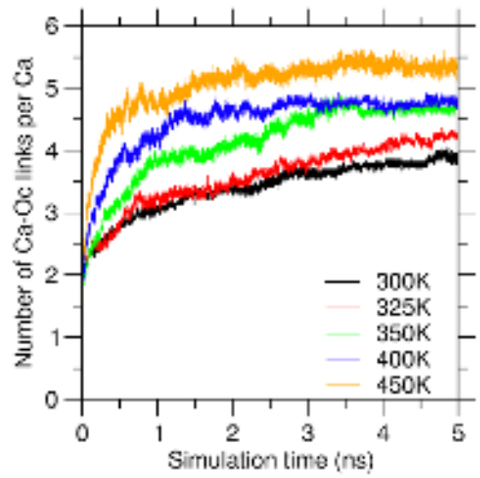

(d) Ca/H_2O=15%

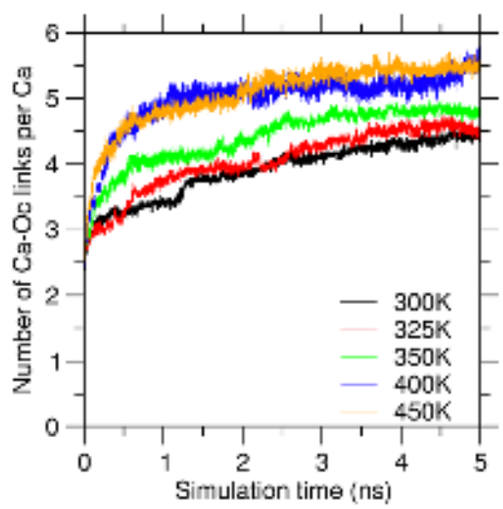

(e) Ca/H_2O=20%

Fig. 3. Number of Ca-Oc cluster at various temperature.

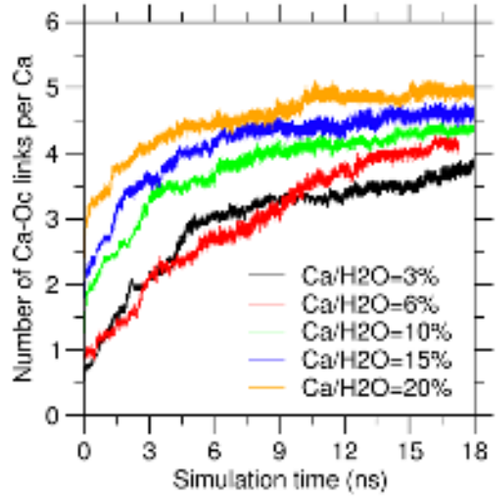

Fig. 4. Number of Ca-Oc cluster at various concentration.

B. Number and size of carbonate cluster

As depicted in Fig. 2~Fig. 4, the formation of Ca-Oc-C bonds gives rise to the emergence of carbonate clusters. Within these clusters, some C atoms are interconnected through Ca atoms, forming the C-Oc-Ca-Oc-C bond. Fig. 5 and Fig. 6 illustrate the number and size of carbonate clusters over time at different calcium concentrations, maintaining a temperature of 300K. Initially, the system comprises numerous isolated small clusters. However, as the simulation progresses, the calcium carbonate gels gradually polymerize, leading to a reduction in the number of carbonate clusters (Fig. 5), accompanied by an increase in the average and maximum sizes of these clusters (Fig. 6). This trend indicates that the carbonate gelation process follows a percolative nature[30]. Moreover, we can also find that the number of calcium carbonate gels eventually decreases and the size becomes larger with the increase of calcium concentration, resulting in the formation of calcium carbonate gel clusters with higher polymerization degree. Therefore, it proves again that the increase of calcium concentration can increase the polymerization rate and degree of calcium carbonate gel, which was in agreement with the result shown in Fig. 4. The number and size of carbonate cluster at different temperature (the Ca/H_2O=3%) are shown in Fig. 7 and Fig. 8. It can be found that the number of calcium carbonate gels

decrease and the size becomes larger with the increase of temperature. Therefore, the increase of temperature can increase the polymerization rate and degree of calcium carbonate gel, which was consistent with the result shown in Fig. 3. Compare Fig. 7 and Fig. 8 to Fig. 5 and Fig. 6, we can find that the increase of temperature makes the calcium carbonate gel reach a relatively large stable size and a smaller quantity in a very short simulation time in comparison with the increase of calcium concentration, which means that the effect of temperature on the polymerization of calcium carbonate gel is greater than that of concentration.

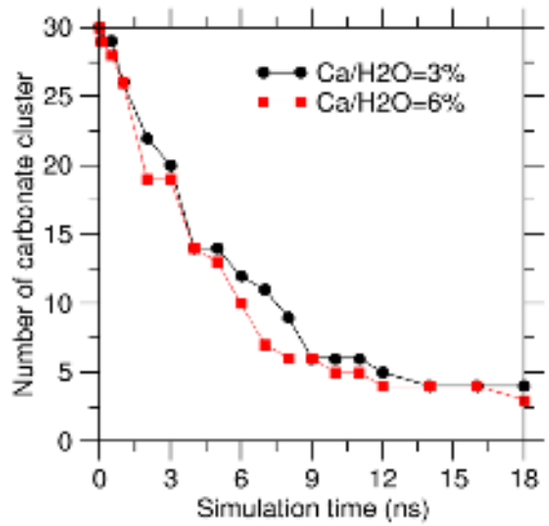

Fig. 5. Number of carbonate cluster at different concentration.

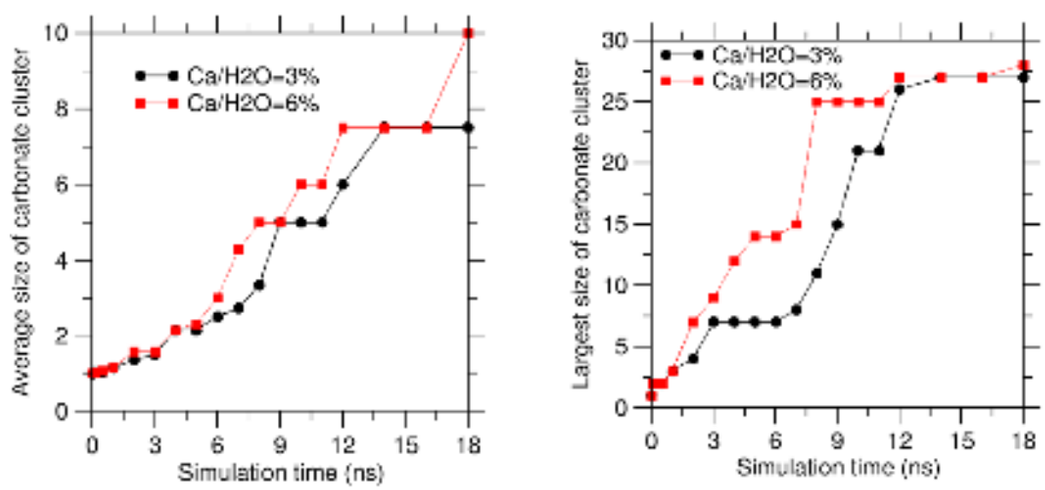

(a) Average size (b) Largest cluster size

Fig. 6. Size of carbonate cluster at different concentration.

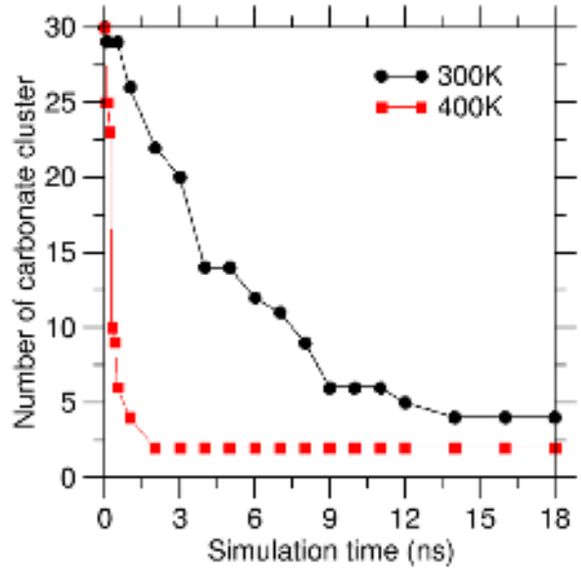

Fig. 7. Number of carbonate cluster at different temperature.

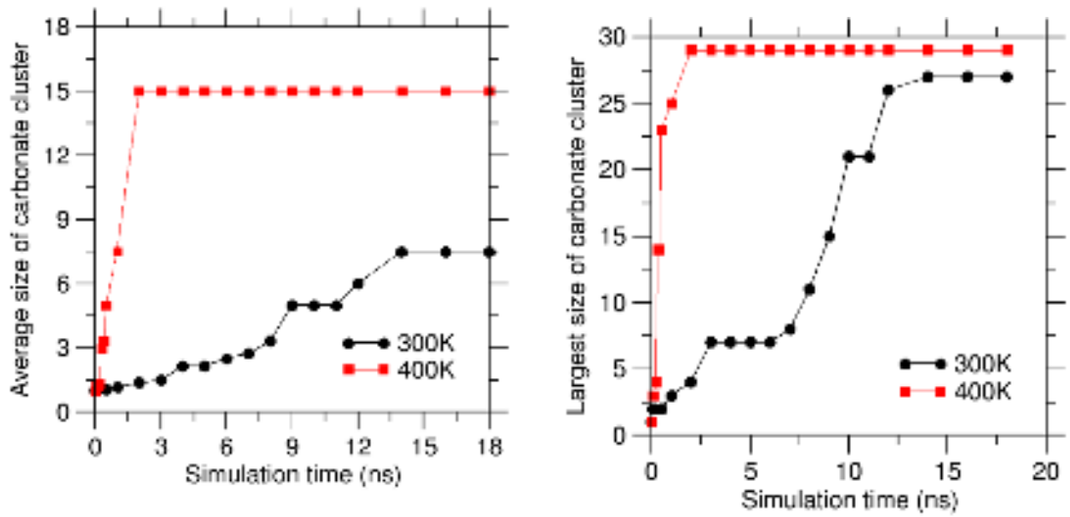

(a) Average size (b) Largest cluster size

Fig. 8. Size of carbonate cluster at different temperature.

The snapshot of the simulated amorphous calcium carbonate system at different simulation time is shown in Fig. 9, for clarity, water molecules are omitted in these snapshots. According to Fig. 9(a), the Ca^{2+} is isolated in the initial configuration. With the prolonging of simulation time, the C-Oc-Ca-Oc-C bonds formed and CO_3^{2-} clusters are connected by Ca atoms, leading to the increase of polymerization degree of calcium carbonate gel. Compared Fig. 9 (d)~(e) with Fig. 9 (b)~(c), the

increase of calcium concentration resulting in the higher polymerization degree of calcium carbonate gel. Moreover, according to Fig. 9 (f)~(g) and Fig. 9 (b)~(c) the higher temperature caused a higher calcium carbonate polymerization degree. Those phenomena are consistent with the result shown in Fig. 3~Fig. 8.

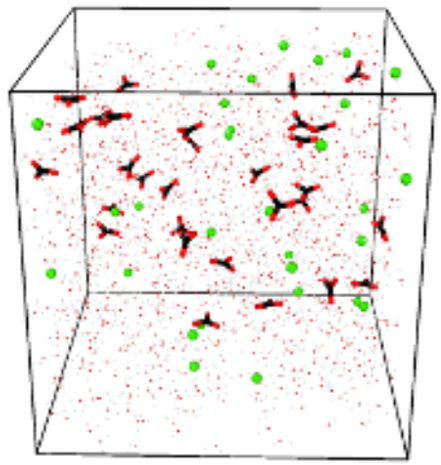

(a) Initial configuration-3% Ca/H_2O

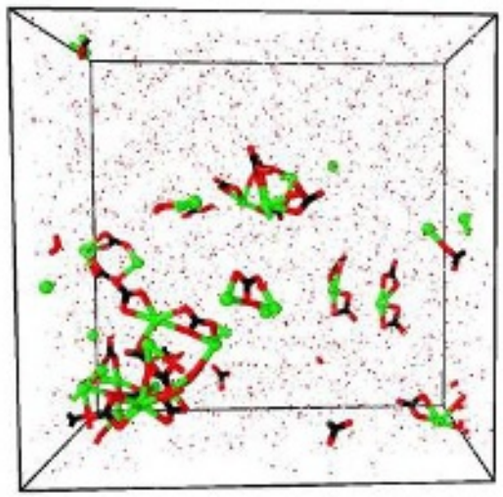

(b) 7 ns-300K-3% Ca/H_2O

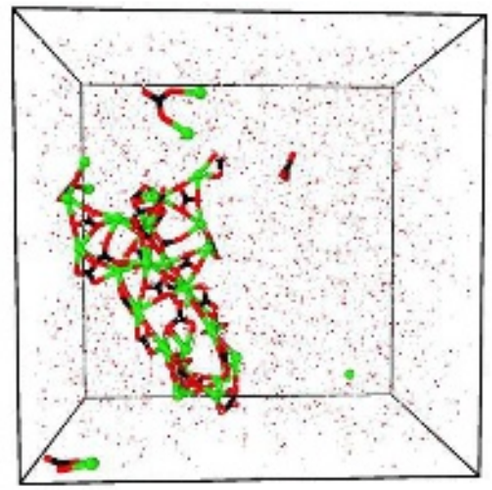

(c) 16 ns-300K-3% Ca/H_2O

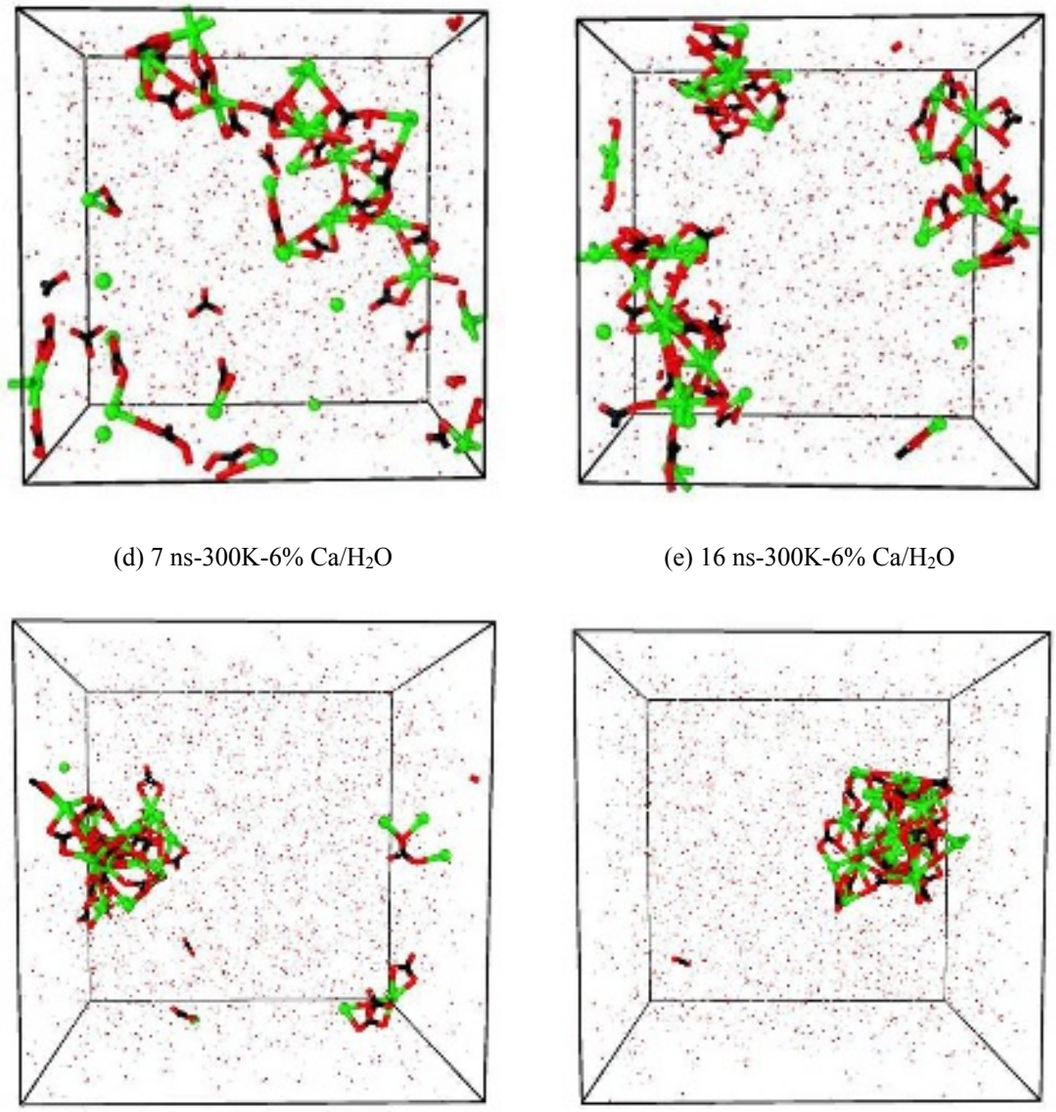

(d) 7 ns-300K-6% Ca/H_2O (e) 16 ns-300K-6% Ca/H_2O

(f) 0.5 ns-400K-3% Ca/H_2O (g) 7 ns-400K-3% Ca/H_2O

Fig. 9. Snapshots of the simulated amorphous calcium carbonate system at various nanoseconds after gelation.

C. Polymerization kinetics

To characterize the reaction kinetics involved in the calcium carbonate condensation process, an investigation into the polymerization process of $CaCO_3$ gel is conducted. Fig. 3, as previously discussed, illustrates the number of Ca-Oc bonds at various calcium concentrations and reaction temperatures. Through the fitting of Ca-Oc(t) curves at various temperatures in Fig. 3, the

polymerization rate is derived. The fitting curves follow an exponential first-order relaxation function, expressed as follows:

$$Ca\text{-}Oc/Ca(t)=A[1-\exp(-kt)] \quad (2)$$

Here, A and k represent the final value of Ca-Oc/Ca molar ratio at infinite simulation time and the polymerization rate coefficient, respectively. Fig. 10 shows the fitting results of calcium carbonate gel polymerization rates at different temperatures and calcium concentrations. It can be found that the calculated value of polymerization rate K increases with the increase of temperature, and it remains an Arrhenius-like dependence on temperature T, regardless of the calcium concentrations. Moreover, the polymerization rate increases with the increase of calcium concentration. That's because the average distance between Ca^{2+} and CO_3^{2-} ions becomes smaller with the increase of calcium concentration, therefore, the probability of collision between Ca^{2+} and CO_3^{2-} ions increases, leading to the increase of polymerization rate[57]. Additionally, our observations include a decrease in the slope of the Arrhenius curves in Fig. 10 with an increase in calcium concentrations. This implies that the energy barrier of the calcium carbonate condensation reaction decreases as calcium concentrations increase. The activation energy (E_A) can be calculated using the following Arrhenius function[58]:

$$k(t)=k_0 \bullet \exp(-E_A/RT) \quad (3)$$

Here, T represents the temperature, R represents the perfect gas constant, k_0 represents the polymerization rate at infinite temperature.

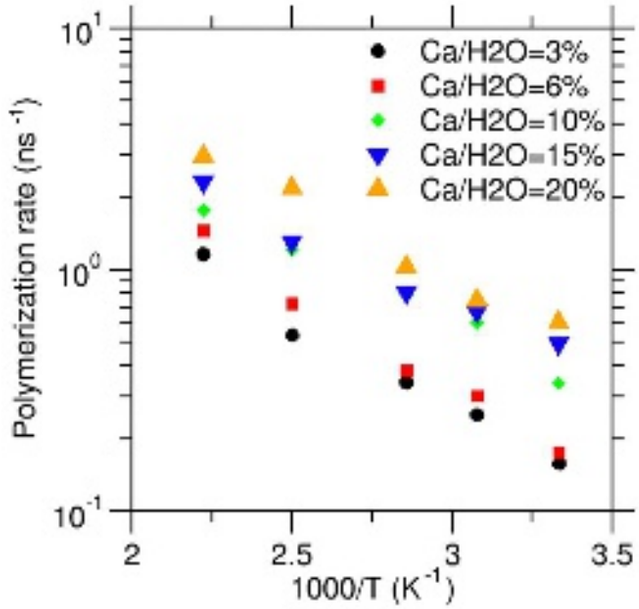

Fig. 10. Polymerization rate of carbonate cluster.

Fig. 11 shows the activation energies of carbonation reaction obtained under different calcium concentrations. The results show that the activation energies of carbonate is 6.63 kJ/mol when the Ca/H2O molar ratio is 3%, which is in accordance with the experiment data (6~7 kJ/mol)[12, 59]. Therefore, the ReaxFF molecular dynamics simulation can well estimate the condensed energy barrier of calcium carbonate gel, thus providing a realistic description of carbonation kinetics. We can also find that the activation energies of carbonation reaction increase with the decrease of calcium concentrations, which indicates that water molecules act as steric hindrance to block the polymerization of calcium carbonate gel[57].

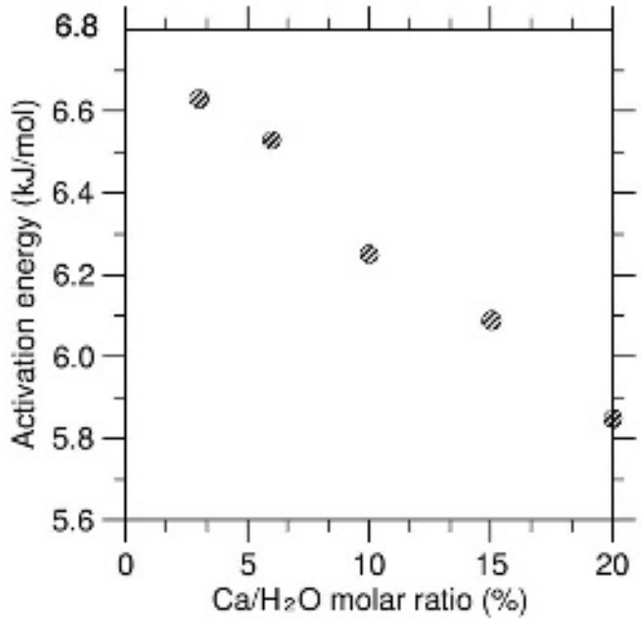

Fig. 11. Activation energy of carbonate cluster various concentration.

D. Local stress

In this section, in order to examine the local stability of the structure, the local stress of each atom in calcium carbonate gel structure is calculated. The local stress evolution of Ca, Ow, C and Oc atoms at different temperatures is presented in Fig. 12. The control values of Ca, C and Oc atoms in Fig. 12 are the corresponding simulated stress values in the pure $CaCO_3$ crystal, respectively. The control value of Ow atom is the simulated stress value of O atom in pure water. It can be found from Fig. 12 (a), (b) that the Ca atoms are in a local tension state (positive stress), nevertheless, the Ow atoms are in a compression state (positive stress). The observed phenomenon can be rationalized by considering the quantity of neighboring water molecules encircling the Ca atom. Fig. 13 illustrates the pair distribution function of O-O surrounding Ca and C-O at 300K. Analysis of Fig. 13(a) reveals that the mean distance between O-O pairs around Ca^{2+} is 2.725 Å, consistent with experimental findings reported in[32] and shorter than the bulk water value of 2.80 Å as documented in[60]. This indicates that adjacent water molecules are drawn closer together due to their attraction to the central calcium ion, resulting in a

locally compressed state. Conversely, repulsive forces among the water molecules exert a tensile effect on the central Ca atom. These opposing local tensile and compressive forces maintain the metastability of the CaO_6 polytope. Notably, the tensile state exhibited by Ca atoms is analogous to that seen in silicate glass, where Si atoms also undergo local tensile stresses[54]. Furthermore, the pH value and calcium concentration of the solution[36] influence the coordination number of Ca atoms, subsequently altering their stress state. Therefore, the impact of solution chemistry on the stress state of gel precursors warrants further investigation. Similarly, it can be seen from Fig. 12 (c) and (d) that C and Oc are in the state of stretching and compression, respectively. According to Fig. 13 (b), the average distance of C-O around carbon atom is 1.275 Å, which is consistent with the experimental data[32] and is significantly shorter than the 1.56 Å[61] in the equilibrium state. Therefore, there is an obvious mutual Coulomb repulsion between the O atom around the C atom, resulting in the C atom being in a state of tension, while the Oc atom is in a state of compression. The entire CO_3 polytope remains metastable.

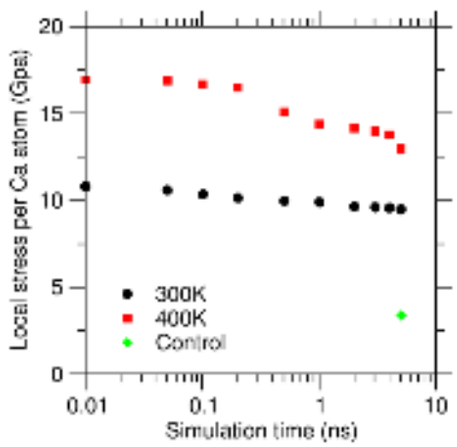

(a) Ca

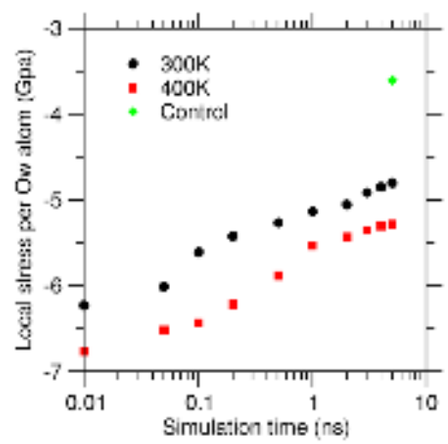

(b) Ow

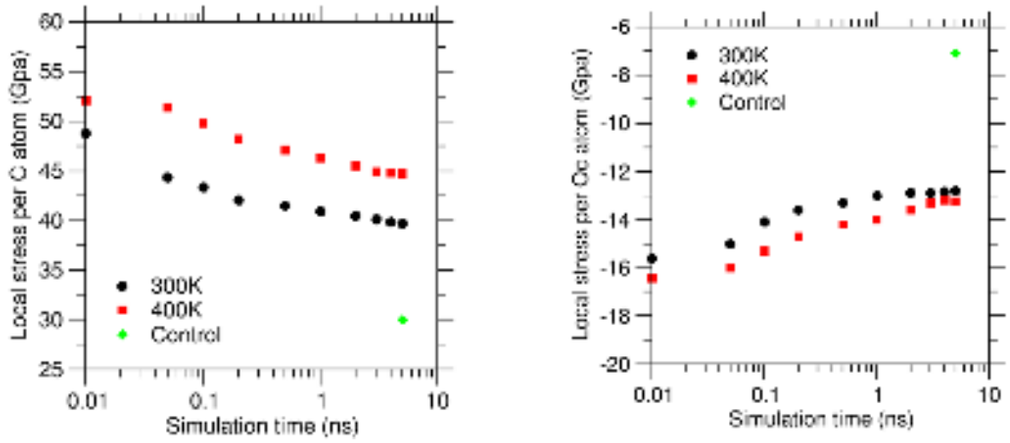

(c) C (d) Oc

Fig. 12. Local stress of Ca, Ow, C, Oc atoms at various temperature.

The results show that despite the overall gel being under zero pressure, there exist local compressive and tensile stresses at the atomic level. This arises from the significant disparity in the coordination numbers of C and Ca atoms. Nevertheless, as evident from Fig. 12, this internal stress is progressively relieved throughout the gelation process. Specifically, the tensile/compressive stress experienced by each atom gradually diminishes and approaches the control value. To investigate the mechanism of local stress relief, we analyze the evolution of the O-O adjacency distance distribution surrounding both Ca and C atoms. As shown in Fig. 13(a) and Fig. 13(c), it is observed that the distributions become increasingly sharper over time, indicating the calcium carbonate gel's increasing stability[30]. Examination of Fig. 13(a) reveals that the average O-O distance around Ca ions experiences a slight increase over time. This trend aligns with the decreasing compression stress on the O atoms neighboring the calcium ions, indicating that the water molecules gradually separate and overlap less with each other. Additionally, the slight increase in the average C-Oc distance (Fig. 13(b)) and O-O distance around C ions (Fig. 13(c)) corroborates the decreasing compression stress experienced by the O atom around the C atom over time. These observations provide insights into the stress relaxation mechanisms within the calcium carbonate gel, which are crucial for understanding its overall stability

and performance.

To further investigate the release of local tensile stress experienced by Ca atoms, we compute the partial pair distribution function of Ca-Ow and Ca-Oc, as depicted in Fig. 13(d) and Fig. 13(e), respectively. The obtained average Ca-O distance in Fig. 13 aligns well with previous experimental findings[32,62-63]. Our observations reveal that the average length of the Ca-Ow bond decreases over time (Fig. 13(d)), whereas the average Ca-Oc bond length increases (Fig. 13(e)). Eventually, distinct types of Ca-O bonds exhibit varying lengths; specifically, the average length of the Ca-Oc bond is greater than that of the Ca-Ow bond. This suggests that the CaO_6 polytope becomes increasingly asymmetric and less spherical. The decoupling between Ca-Ow and Ca-Oc bond lengths underlies the increasing O-O distance around the Ca atom (Fig. 13(a))[30]. Overall, the average length of the Ca-O bond decreases over time due to the predominance of Ca-Ow bonds, indicating that the central Ca atom experiences less stretching over time. Therefore, these findings indicate that the formation of Ca-O-C bonds (calcium carbonation clusters) directly contributes to the reduction of local stress exhibited by Ca atoms. Analogous behavior has been observed in calcium aluminosilicate hydrate gels, where Si-O-Al bond formation has been shown to mitigate internal stress in Si (locally stretched) and Al (locally compressed) precursors[64]. This suggests that the relationship between gelation and local internal stress may be generalizable to various hydration systems[57,64].

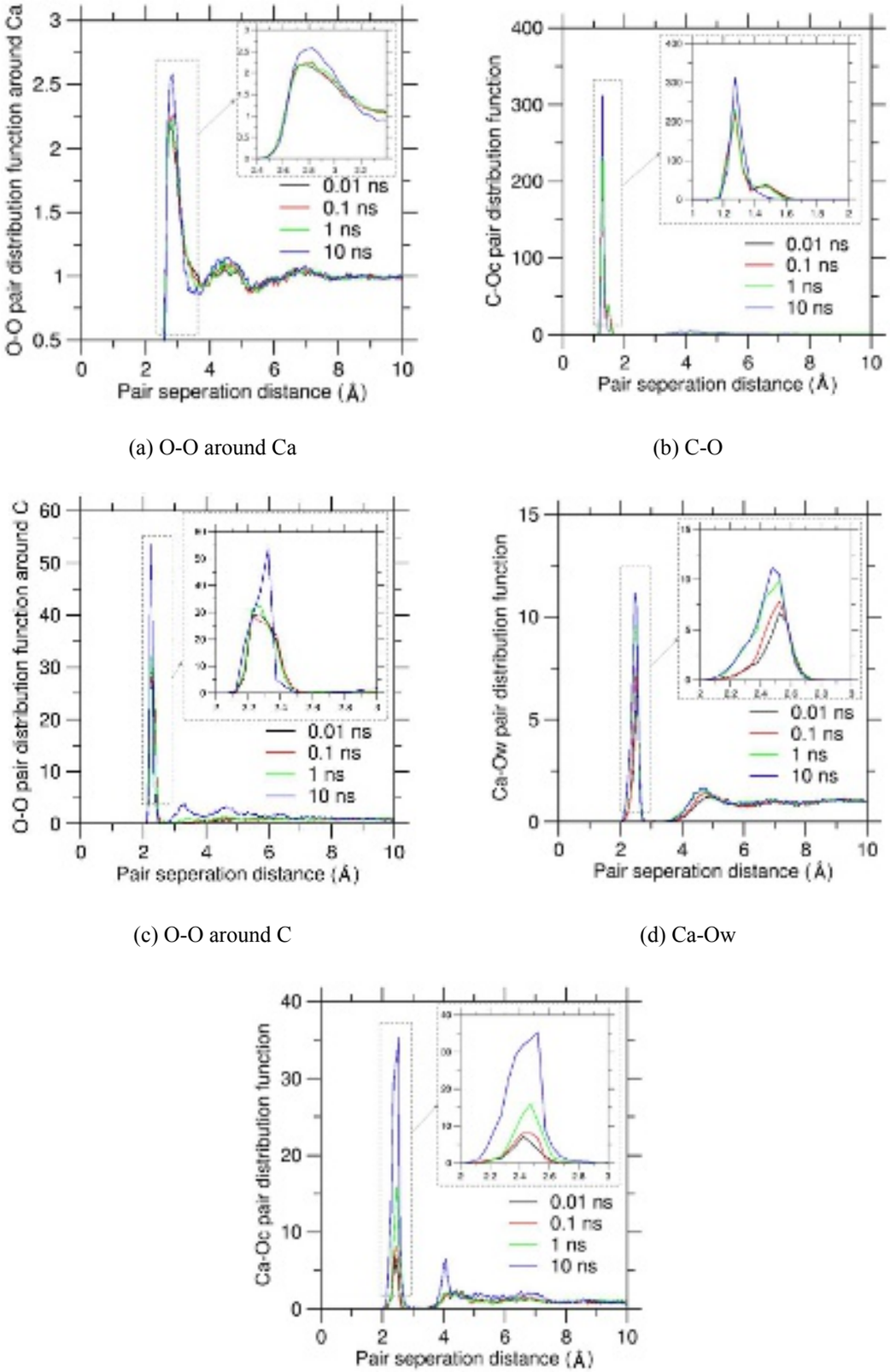

(a) O-O around Ca

(b) C-O

(c) O-O around C

(d) Ca-Ow

(e) Ca-Oc

Fig. 13. Pair distribution function.

According to the discussion above, the initial local stress in the system is the driving force of gel transformation, and the higher the local stress is, the higher the polymerization rate of calcium carbonate will be. It can also be seen from Fig. 12 that the higher the temperature, the greater the local stress of the atom, which is in agreement with the conclusion that the increase of the temperature can promote the polymerization rate of calcium carbonate gel as present in Fig. 10. Fig. 14 presents the local stresses of Ca, Ow, C, and OC atoms at different of calcium concentration when the temperature is 300 K and simulation time is 10 ns. We can find that the final local stress of each atom increases with the increase of calcium concentration. Therefore, the polymerization rate of the calcium carbonate gel is increase, which is also consistent with the results presented in Fig. 10.

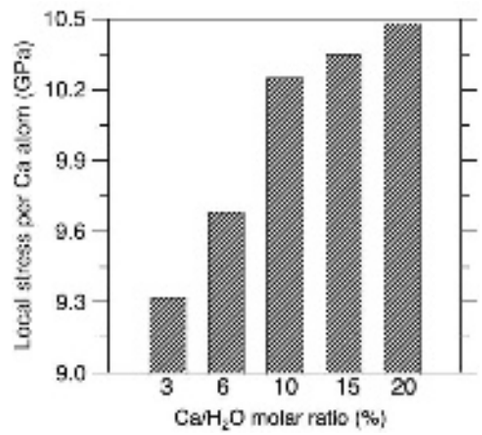

(a) Ca

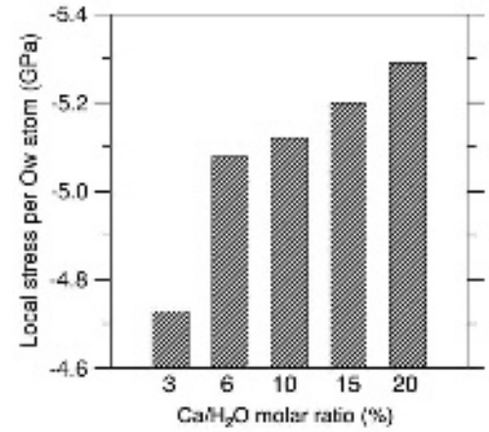

(b) Ow

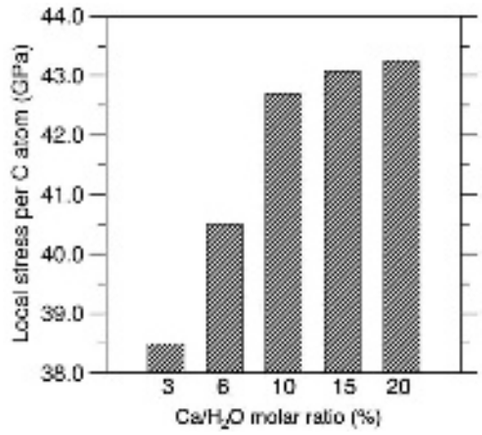

(c) C

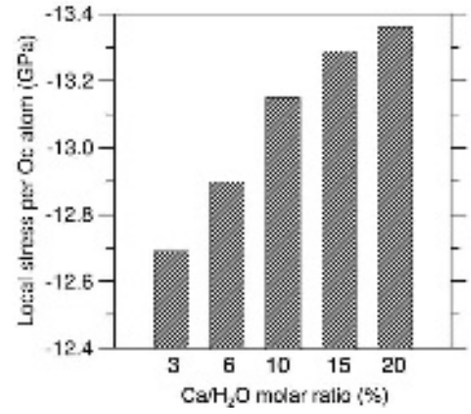

(d) Oc

Fig. 14. Local stress of Ca, Ow, C, Oc atoms at various concentration.

IV. CONCLUSIONS

This study delves into the implications of temperature variations and CO_2 concentration levels on the initial nucleation stage of calcium carbonate during the carbonation curing process of cementitious materials. The objective is to enhance the mineralization capture, stabilization, and utilization of carbon dioxide, thereby laying a robust scientific groundwork for a process that has hitherto relied primarily on empirical knowledge. This approach aims to contribute to the development of innovative cementitious materials that offer superior performance while being more environmentally friendly. In summary, the simulation results lead to the following conclusions.

(1) An elevation in temperature or Ca^{2+} concentration results in an augmentation of the polymerization rate and degree of calcium carbonate, alongside a concurrent reduction in the activation energy required for its polymerization reaction. Notably, the influence of temperature on calcium carbonate gel polymerization is more pronounced than that of concentration.

(2) Despite the overall system being maintained at zero pressure, the initial stages of the polymerization process witness competing internal stresses within the CaO_6 and CO_3 polytope precursors. The local stress of each atom in the system is the driving force of the gel transformation. The local stress of the atoms is gradually released (the tensile/compressive stress of each atom is gradually reduced) with the progress of calcium carbonate gel gelation.

(3) The larger the local stress is, the higher the polymerization rate of calcium carbonate will be. The local stress of atoms increases with the increase of temperature and Ca^{2+} concentration, therefore, leading to the higher polymerization rate of calcium carbonate.

(4) The atomical scale mechanism of carbonation in magnesium base cementitious material is still

unclear and will be studied in the future

ACKNOWLEDGMENTS

This research was supported by the National Key Research and Development Program of China (Grant No. 2021YFB2600704), the National Natural Science Foundation of China (Grant No. 52208260, U23A20661, 52341803), the Natural Science Foundation of Shandong province (Grant No. ZR2022QE002), the National Science Foundation (Grant No. DMREF-1922167) and the China Postdoctoral Science Foundation (Grant No. 2023MD734207), the Youth Innovation Team Development Plan of Shandong Province in China (2023KJ113).

AUTHOR DECLARATIONS

Credit authorship contribution statement

Ling Qin: Writing – original draft; Investigation; Methodology. Junyi Yang: Writing – review & editing. Jiuwen Bao: Writing – review & editing. Gaurav Sant: Writing – review & editing. Sheng Wang: Writing – review & editing. Peng Zhang: Funding acquisition; Writing – review & editing. Xiaojian Gao: Writing – review & editing. Qi Yu: Writing – review & editing. Ditao Niu: Writing – review & editing. Mathieu Bauchy: Writing – review & editing; Funding acquisition; Supervision.

Declaration of competing interest

The authors declare that they have no known competing financial interests or personal relationships that could have appeared to influence the work reported in this paper.

DATA AVAILABILITY

Data will be made available upon reasonable request.

REFERENCES

[1]B. Zhan, C. Poon, and C. Shi, Cem. Concr. Compos. 42, 1 (2013).

[2]A. Deepak, V. Sharma, and D. Kumar, J. clean. Prod. 349 (2022).

[3]J.J. Biernacki, J.W. Bullard, G. Sant, K. Brown, F.P. Glasser, S. Jones, T. Ley, R. Livingston, L. Nicoleau, J. Olek, F. Sanchez, R. Shahsavari, P.E. Stutzman, K. Sobolev, and T. Prater, J. Am. Ceram. Soc. 100.7, 2746 (2017).

[4]M.F. Kai, L.W. Zhang, and K. M. Liew, Carbon. 146, 181-193 (2019).

[5]A.M. Tawfek, Z. Ge, H. Yuan, N. Zhang, H. Zhang, Y. Ling, Y. Guan, and B. Šavija, J. Build. Eng. 63 (2023).

[6]M.F. Kai, L.W. Zhang, and K. M. Liew, Cem. Concr. Res. 142, 106366 (2021).

[7]G. Habert, S.A. Miller, V.M. John, J. Provis, A. Favier, A. Horvath, and K.L. Scrivener, Nat. Rev. Earth Env. 1.11, 559 (2020).

[8]R.M. Andrew, Earth Syst. Sci. Data. 10.1, 195 (2018).

[9]R.K. Pachauri, M.R. Allen, and V.R. Barros, et al., J. Romanc. Stud. 4.2, 85 (2014).

[10]B. Bajželj, J.M. Allwood, and J.M. Cullen, Environ. Sci. Technol. 47.14, 8062 (2013).

[11]S.A. Miller, V.M. John, S.A. Pacca, and A. Horvath, Cem. Concr. Res. 114, 115 (2018).

[12]K. Vance, G. Falzone, I. Pignatelli, M. Bauchy, M. Balonis, and G. Sant, Ind. Eng. Chem. Res. 36, 8909 (2015).

[13]Z. Giergiczny, A. Król, M. Tałaj, and K. Wandoch, 13.17, 4328 (2020).

[14]V. Rostami, Y. Shao, and A.J. Boyd, Constr. Build. Mater. 25.8, 3345 (2011).

[15]Z. Šauman, Cem. Concr. Res. 1.6, 645 (1971).

[16]L. Qin, and X. Gao, Fuel. 245, 1 (2019).

[17]L. Qin, and X. Gao, Waste Manage. 89, 254 (2019).

[18]L. Qin, X. Gao, and T. Chen, Constr. Build. Mater. 212, 653 (2019).

[19]L. Qin, X. Gao, A. Su, and Q. Li, J. Clean. Prod. 278, 123897 (2021).

[20]T. Chen, and X. Gao, J. CO_2 Util. 34, 74 (2019).

[21]M.Á. Sanjuán, E. Estévez, C. Argiz, and D. Barrio, Cem. Concr. Comp. 90, 257 (2018).

[22]D.C. Johnson, C.L. MacLeod, P.J. Carey, and C.D. Hills, Environ. Technol. 24.6, 671 (2003).

[23]J. Chang, Y. Fang, and X. Shang, Mater. Struct. 49, 4417 (2016).

[24]S. Kashef-Haghighi, Y. Shao, and S. Ghoshal, Cem. Concr. Res. 67, 1 (2015).

[25]C. Shi, M. Liu, P. He, and Z. Ou, 1.1-2, 24 (2012).

[26]M.A. Sanjuan, C. Andrade, and M. Cheyrezy, Adv. Cem. Res. 15.4, 171 (2003).

[27]W. Ashraf, and J. Olek, J. Mater. Sci. 51, 6173 (2016).

[28]J.M. Bukowski, and R.L. Berger, Cem. Concr. Res. 9.1, 57 (1979).

[29]Y.W. Wang, Y.Y. Kim, C.J.Stephens, F.C. Meldrum, and H.K. Christenson, Cryst. Growth Des. 12.3, 1212 (2012).

[30]Q. Zhou, T. Du, L. Guo, G. Sant, and M. Bauchy, Appl. Sci. 10.12, 4359 (2020).

[31]M.G. Taylor, K. Simkiss, G.N. Greaves, M. Okazaki, and S. Mann, P. Roy. Soc. B-Biol. Sci. 252, 75 (1993).

[32]F.M. Michel, J. MacDonald, J. Feng, B.L. Phillips, L. Ehm, C. Tarabrella, J.B. Parise, and R.J. Reeder, Chem. Mater. 20, 4720 (2008).

[33]K. Henzler, E.O. Fetisov, M. Galib, M.D. Baer, B.A. Legg, C. Borca, J.M. Xto, S. Pin, J.L. Fulton, and G.K. Schenter, et al., Sci. Adv. 4, eaao6283 (2018).

[34]S. Plimpton, J. Comput. Phys. 117, 1 (1995).

[35]A. Pallagi, Á. Tasi, A. Gácsi, M. Csáti, I. Pálinkó, G. Peintler, and P. Sipos, Cent. Eur. J. Chem. 10, 332 (2012).

[36]J. Avaro, E.M. Moon, J. Rose, A.L. Rose, Geochim. Cosmochim. Ac. 259, 344 (2019).

[37]P.J. Smeets, A.R. Finney, and W.J Habraken, et al., P. Natl. Acad. Sci. USA. 114, E7882 (2017).

[38]L. Martínez, R. Andrade, E.G. Birgin, and J.M. Martínez, J. Comput. Chem. 30, 2157 (2009).

[39]W. Shinoda, M. Shiga, and M. Mikami, Phys. Rev. B 69, 134103 (2004).

[40]M.E. Tuckerman, J. Alejandre, R. López-Rendón, A.L. Jochim, and G.J. Martyna, J. Phys. Math. Gen. 39, 5629 (2006).

[41]J.D. Gale, P. Raiteri, and A.C. Van Duin, Phys. Chem. Chem. Phys. 13, 16666 (2011).

[42]L. Qin, X. Mao, Y. Cui, J. Bao, G. Sant, T. Chen, P. Zhang, X. Gao, and M. Bauchy, J. Chem. Phys. 157, 234501 (2022).

[43]E. Demiralp, T. Çağin, and W.A. Goddard III, Phys. Rev. Lett. 82, 1708 (1999).

[44]M.F. Kai, F. Sanchez, D.S. Hou, and J.G. Dai, Appl. Surf. Sci. 616, 156478 (2023).

[45]M.F. Kai, D.S. Hou, F. Sanchez, C.S. Poon, and J.G. Dai, J. Phy. Chem. C. 127.18, 8735 (2023).

[46]P. Raiteri, R. Demichelis, and J.D. Gale, J. Phys. Chem. C 119, 24447 (2015).

[47]A.C. Van Duin, A. Strachan, S. Stewman, Q. Zhang, X. Xu, and W.A. J. Phys. Chem. A 107, 3803 (2003).

[48]A.C. Van Duin, S. Dasgupta, F. Lorant, and W.A. Goddard, J. Phys. Chem. A 105, 9396 (2001).

[49]A. Stukowski, Model. Simul. Mater. Sc. 18, 015012 (2009).

[50]V. Vitek, and T. Egami, Phys. Status Solidi B. 144, 145 (1987).

[51]T. Egami, Prog. Mater. Sci. 56, 637 (2011).

[52]A.P. Thompson, S.J. Plimpton, and W. Mattson, J. Chem. Phys. 131, (2009).

[53]Y. Yu, M. Wang, N.M. Anoop Krishnan, M.M. Smedskjaer, K. Deenamma Vargheese, J.C. Mauro, M. Balonis, and M. Bauchy, J. Non-Cryst. Solids. 489, 16 (2018).

[54]X. Li, W. Song, M.M. Smedskjaer, J.C. Mauro, and M. Bauchy, J. Non-Cryst. Solids X. 1, 100013 (2019).

[55]M.F. Kai, and J.G. Dai, Cem. Concr. Res. 149, 106582 (2021).

[56]M.F. Kai, W. Ji, and J.G. Dai, Eng. Fract. Mech. 271, 108668 (2022).

[57]T. Du, H. Li, G. Sant, and M. Bauchy, J. Chem. Phys. 148, (2018).

[58]S.G.E. Giap, J. Phys. Sci. 21, 29 (2010).

[59]G. Montes-Hernandez, R. Chiriac, F. Toche, and F. Renard, Int. J. Greenh. Gas Con. 11, 172 (2012).

[60]J. Mahler, and I. Persson, Inorg. Chem. 51, 425 (2012).

[61]R.D. Shannon, Acta Crystallogr. Sect. A 32, 751 (1976).

[62]A. Becker, U. Bismayer, M. Epple, H. Fabritius, B. Hasse, J. Shi, and A. Ziegler, Dalton Trans. 4, 551 (2003).

[63]Y. Levi-Kalisman, S. Raz, S. Weiner, L. Addadi, and I. Sagi, Adv. Funct. Mater. 12, 43 (2002).

[64]C. Zhao, W. Zhou, Q. Zhou, Y. Zhang, H. Liu, G. Sant, X. Liu, L. Guo, and M. Bauchy, J. Chem. Phys. 153, (2020).